ISABE-2005-1168

ROLE OF CFD IN THE AERODYNAMIC DESIGN AND ANALYSIS OF THE PARAMETRIC INLET

John W. Slater* *and* David O. Davis*
NASA John H. Glenn Research Center at Lewis Field, Brook Park, Ohio 44135 USA

and

Bobby W. Sanders† *and* Lois J. Weir‡
TechLand Research, Inc., North Olmsted, Ohio 44070 USA

Abstract

Computational Fluid Dynamics (CFD) played a significant role in the design of the Parametric Inlet – an advanced, external-compression, supersonic inlet. CFD allowed the designers to account for turbulent boundary layers and shock / boundary-layer interactions during the design of the shape of the internal inlet surfaces, define locations of porous bleed regions, optimize porous bleed factors, examine the effect of a vortex generator array, and examine inlet configurations with various cowl and slot geometries. The CFD simulations provided information that allowed the efficient use of costly wind tunnel resources. Preliminary comparisons between CFD and experimental data are encouraging for the validation of CFD methods for supersonic inlet design.

Nomenclature

DPCPAV	ring-average of circumferential distortion
p_{corner}	static pressure of the corner bleed plenum
p_{slot}	static pressure of the slot plenum
Φ_{aft}	porosity of the aft bleed region
W_2	engine flow
W_{bleed}	bleed flow
W_{cap}	ideal capture flow
$W_{spillage}$	spillage flow

Introduction

The challenge of developing an efficient propulsion system for commercial aircraft supersonic cruise has been a research topic for over 40 years.[1] A central component of such a propulsion system is the inlet, which captures a portion of the supersonic freestream air and then decelerates and compresses the air to subsonic speeds for delivery to a turbofan engine. The flow is characterized by oblique and normal shock waves that interact with turbulent boundary layers on the surfaces of the inlet. Since the inlet is a flow compression device, the flow field has an adverse pressure gradient. These set up conditions for boundary-layer separation. A primary objective of a supersonic inlet design is to minimize or eliminate separation so as to provide airflow to the engine that has minimal losses and low levels of distortion.

The Parametric Inlet is a recent, advanced concept for a supersonic inlet. It was developed by TechLand Research, Inc. and the NASA John H. Glenn Research Center (NASA-GRC) and then fabricated and tested in the NASA-GRC 10-foot-by-10-foot supersonic wind tunnel (SWT). The Parametric Inlet was designed for SWT test section conditions of a Mach 2.35 flow field at a Reynolds number per foot of 2.5E+06. The engine face diameter was 16.07 inches. Figure 1 shows the Parametric Inlet mounted in the SWT along with a schematic showing the half-plane computational model with the salient features of the inlet identified.

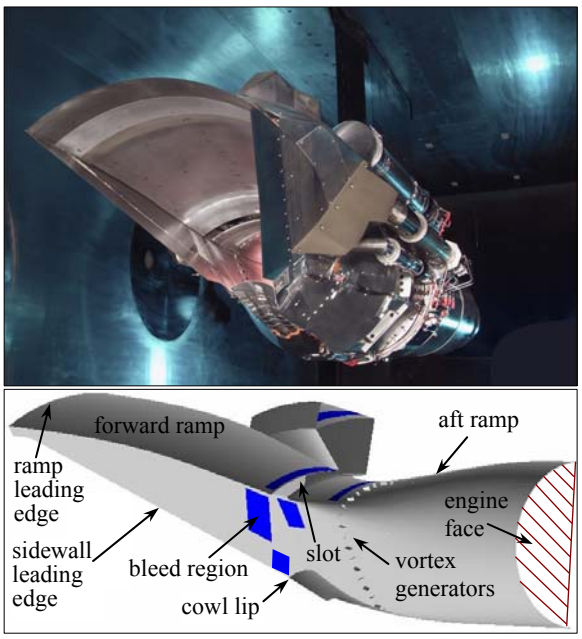

Figure 1. The Parametric Inlet in the NASA-GRC 10-ft-by-10-ft supersonic wind tunnel (top) and as a half-plane computational model for CFD simulations (bottom).

The Parametric Inlet is an external-compression inlet for which the terminal shock exists ahead of the cowl lip in a sub-critical supersonic condition. Upstream of the terminal shock is the supersonic

* Aerospace Engineer, Inlet Branch. † President. ‡ Chief Executive Officer.

diffuser for which the flow is supersonic. Downstream of the terminal shock is the subsonic diffuser for which the flow is subsonic to the engine face. Since the terminal shock is ahead of the cowl lip, subsonic flow may spill past the cowl lip. The choice to use external-compression was made after significant experience with the design and testing of mixed-compression inlets as part of the NASA High Speed Research program of the 1990s.[1] The concept of the Parametric Inlet promised aerodynamic performance nearing that of a mixed-compression inlet, but without the mechanical complexity and concern about flow instability. The primary instability of mixed-compression inlets has been the possibility of inlet unstart in which the terminal shock is expelled from the inlet with the result of a severe unbalance of forces. The innovative feature of the Parametric Inlet is that the supersonic, conical flow field is turned inward toward the axis-of-symmetry. One disadvantage of past designs of external-compression inlets was the relatively high level of cowl drag. By turning the flow inward, the external area of the cowl lip is reduced, which reduces the cowl drag. The inlet has forward and aft ramps that pivot to allow the throat area to vary to adjust the inlet flow to freestream conditions. The forward ramp is part of the supersonic diffuser. The aft ramp is part of the subsonic diffuser. A slot is located at the throat which physically separates the forward and aft ramps. The slot opening also limits harmful interactions between the terminal shock and boundary layers on the ramps. The Parametric Inlet used porous bleed to provide terminal shock stability (stability bleed) and improve performance by improving boundary-layer health (performance bleed). The porous bleed regions consisted of small-diameter circular holes drilled into to the surface. The porosity Φ is the ratio of the sum of the hole area to the area of the bleed region. The bleed holes extract a portion of the boundary-layer flow into a bleed plenum. The bleed flow is extracted from the inlet flow when the inlet flow static pressure exceeds the static pressure of the bleed plenum. The bled flow is then piped away to be dumped into a low-pressure area. The "parametric" aspect of the inlet indicates that a variety of cowl lip and slot geometries were designed that could be interchanged into the inlet configuration as part of the wind tunnel testing. The slot geometries varied the start location and the length of the opening of the slot. The cowl geometries varied the location and angle of the cowl lip. The Parametric Inlet contained a single, circumferential row of vortex generators (VGs) located within the subsonic diffuser. The objective of the VGs was to create vortices that energized the boundary layer to reduce boundary-layer separation. The incidence angle of each VG was set at either a positive or negative incidence to create a array of counter-rotating or co-rotating VGs.

The primary performance measures for a supersonic inlet are the 1) engine flow W_2, 2) bleed flow W_{bleed}, 3) spillage flow $W_{spillage}$, 4) total pressure recovery, and 5) total pressure distortion. The *engine flow* is the amount of the ideal capture flow (W_{cap}) that actually enters the engine. The ideal capture flow W_{cap} is the maximum flow that the inlet would take in under ideal circumstances. The *bleed flow* is the amount of ideal capture flow extracted by the porous bleed systems and the slot. The *spillage flow* is that amount of ideal capture flow that "spills" past the sidewalls and cowl lip. The *total pressure recovery* is the ratio of the average total pressure at the engine face to the freestream total pressure. The loss of total pressure in the flow through the inlet represents a loss in the reversible or recoverable flow energy due to flow through shock waves and turbulent boundary layers. The engine flow and the total pressure recovery can be summarized in a "mass flow characteristic curve", which plots the variation of the total pressure recovery with the engine flow normalized by the ideal capture flow. This characteristic curve is sometimes referred to as the "cane curve" as its shape can resemble a walking cane. The *total pressure distortion* characterizes the level of radial and circumferential total pressure variation at the engine face. A large amount of distortion, especially circumferential distortion, may lead to instabilities within the engine and premature engine fatigue. One measure of circumferential distortion is DPCPAV, which is the algebraic average of the SAE ARP 1420 circumferential distortion intensity element $\Delta PC/P$ for each ring.[2]

Computational Fluid Dynamics (CFD) provided a highly effective tool for the design of the Parametric Inlet through simulation of the inlet flows and evaluation of the performance measures. The next section discusses the CFD methods. CFD design studies were performed concurrently with the mechanical design. This paper discusses those studies and the instances in which the CFD studies resulted in significant design changes not anticipated by the designers when using traditional methods of design. CFD allowed the designers to account for turbulent boundary layers and shock / boundary-layer interactions during the design of the shape of internal inlet surfaces, define locations of porous bleed regions, optimize porous bleed factors, examine the effect of a vortex generator array, and examine inlet configurations with various cowl and slot geometries. The CFD simulations provided information that allowed the efficient use of costly wind tunnel resources. Preliminary comparisons between CFD results and experimental data are presented as a part of the validation of CFD methods for supersonic inlet design.

CFD Methods

The CFD simulations were performed using the Wind-US CFD code.[3] Wind-US is being developed by the NPARC Alliance (National Program for Applications-oriented Research in CFD), which is an alliance of the NASA-GRC, the U.S. Air Force Arnold Engineering Development Center, and the Boeing Company. Wind-US solves the Reynolds-averaged Navier-Stokes equations in a time-dependent manner for turbulent, compressible flows using a cell-vertex, finite-volume, time-marching approach. The simulations were performed using multi-zone, structured grids. Spatial accuracy was formally second-order using the Roe flux-difference splitting upwind formulation. Steady flows were simulated through an iterative process using local time stepping. The supersonic inlet simulations assumed a calorically perfect gas model. The supersonic inflow boundary condition matched the flow conditions of the SWT test section. Turbulence was modeled using the one-equation Spalart-Allmaras model. Porous bleed was modeled as a boundary condition in which the bleed rate could vary according to local flow conditions. The primary inputs for the porous bleed model were the porosity Φ of the bleed region and the static pressure of the plenum for the bleed region. The engine flow was modeled with an attached, choked nozzle zone for startup, but then switched to a mass-flow boundary condition for sweeps of the cane curve. The vortex generators were modeled as flat plates. Reference [4] discussed further details on the CFD methods used for the simulations of the Parametric Inlet.

CFD Design Studies

The following sections discuss several design studies in which CFD played a significant role in the design of the Parametric Inlet.

Axisymmetric Contour of the Supersonic Diffuser

The supersonic diffuser decelerates the Mach 2.35 inflow to a Mach number of Mach 1.3 prior to the terminal shock. Traditional design methods based on compressible flow theory and method of characteristics established a conceptual design consisting of an axisymmetric contour with a conical shock emanating from the leading edge followed by an isentropic compression focused near the ideal cowl lip position. The traditional design methods did not account for the growth of the turbulent boundary layer along the diffuser. CFD methods were used to perform axisymmetric simulations. The terminal shock was not modeled; rather the flow domain was truncated near the throat and an extrapolation boundary condition was applied such that the flow field remained supersonic. Figure 2 shows the Mach number contours of the axisymmetric flow field. The contour of the supersonic diffuser was adjusted to account for boundary layer growth and to tailor the Mach 1.3 line to be straight and located at the end of the forward ramp.

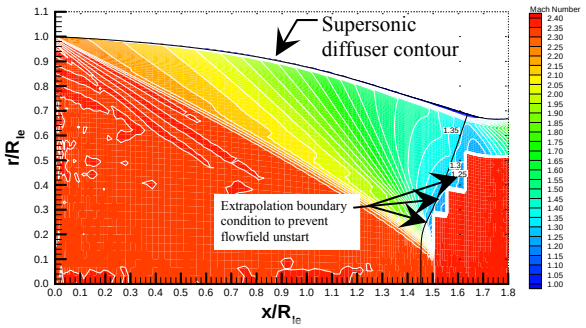

Figure 2. Mach number contours of the axisymmetric flow field of the supersonic diffuser.

Baseline "Clean" Inlet

Once the axisymmetric contour of the supersonic diffuser was established, the three-dimensional shape of the supersonic diffuser, cowl, and subsonic diffuser was generated. The axisymmetric contour was extruded over a 70-degree circumferential sector to form the forward ramp. The cowl was also extruded over a 70-degree sector and fitted with an elliptic leading edge to form the baseline cowl. The sidewalls of the supersonic diffuser were flat with a leading edge formed by a line from the ramp leading edge to the cowl lip. The internal angles of the cowl lip turned the flow to axial. The subsonic diffuser was formed through a transition from a partial annular cross-section at the throat to a circular cross-section at the engine face. The cross-sectional area distribution through the subsonic diffuser was adjusted to provide a smooth increase in area.

The CFD simulations of this geometry established the baseline aerodynamics of the "clean" inlet without bleed, slots, and vortex generators. First, simulations examined a supersonic flow-through of the inlet, which exhibited the minimum spillage flow and the maximum engine flow. A bow shock formed at the cowl lip and there was a small subsonic region around the cowl lip. Simulations were then performed to attempt to establish a terminal shock ahead of the cowl lip and subsonic flow in the subsonic diffuser. The engine flow boundary was modeled using a nozzle zone. As the nozzle throat radius was reduced, the nozzle throat choked and a normal shock formed ahead of the nozzle throat. The normal shock propagated forward in the duct toward the throat. Significant regions of boundary-layer separation developed in the duct due to the shock / boundary-layer interactions. The normal shock was expelled from the duct, but kept moving forward onto the ramp. The CFD simulations demonstrated that some form of flow control was

needed to stabilize the terminal shock. The throat slot and porous bleed regions provided this control.

Baseline Throat Slot and Porous Bleed

The use of a throat slot and porous bleed regions was assumed during the conceptual design of the inlet. Traditional methods were used for the initial placement of the slot, the ramp and sidewall stability bleed regions, and the aft performance bleed region. Only after extensive CFD simulations, was it determined that the slot corner and cowl sidewall bleed regions were needed as additional performance bleed regions. For the CFD simulations, the geometry of the baseline slot was modeled along with an approximation of the slot plenum. To extract the slot flow, a slot bleed region was modeled at the top of the slot plenum using the porous bleed model. Figure 3 shows the slot and the bleed regions of the final configuration. The simulations of this study did not model the vortex generators.

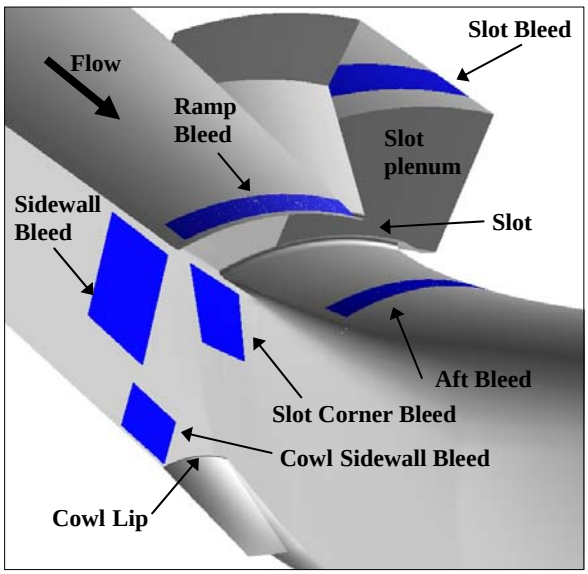

Figure 3. Parametric Inlet bleed regions.

The porosity of the bleed regions was set at 40%, except for the slot bleed region, which was set at 100%. The bleed plenum static pressure for each bleed region was determined by first estimating the value of static pressure in the flow field near the bleed region. The static pressure was then adjusted as subsequent CFD simulations provided greater information on the local flow field and the resulting bleed rate. The setting of the static pressures was compounded by the interactions between the terminal shock, boundary layers, and bleed regions. The terminal shock was formed from the coalescence of the bow shock about the cowl lip with the normal shock expelled from within the subsonic diffuser. As the normal shock moved forward in the subsonic diffuser, the strong shock / boundary-layer interactions resulted in significant boundary-layer separations, which further complicated the establishment of a stable flow field. As the normal shock approached the throat and began to be expelled, its strength was reduced and the bleed regions helped stabilize the terminal shock in the desired position. Stability occurred only if the bleed regions extracted enough flow to stabilize the shock.

Figure 4 shows the Mach number contours on the symmetry plane for a representative simulation with the terminal shock correctly established. A conical shock emanates from the ramp leading edge and the supersonic flow is compressed along the forward ramp. The bow shock about the cowl lip blends nicely with the terminal shock, which is planar and intersects the opening of the throat slot. Downstream of the terminal shock, the flow is subsonic.

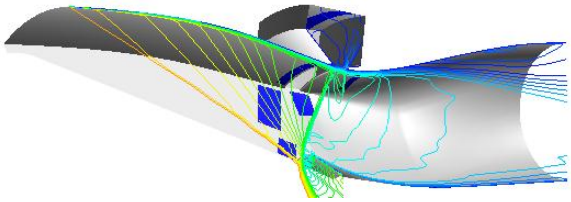

Figure 4. Mach contours on the symmetry plane.

The CFD simulations revealed several items of concern in the flow field and allowed an understanding of how to make changes to the inlet design to address the concerns.

The first item of concern was the extensive boundary-layer separation and reversed flow that developed on the upper surface of the subsonic diffuser. It was concluded that the turning in the subsonic diffuser was too aggressive. The solution was to lower the engine face. This moved the engine face out from the mask of the frontal area of the supersonic diffuser and likely resulted in increased external drag. However, the objective of the wind tunnel tests was to examine the internal flow, and so, the increase of external drag was considered acceptable. CFD simulations indicated that lowering the engine face did reduce the amount and extent of the boundary-layer separation on the upper surface of the subsonic diffuser; however, significant separation still existed.

A second item of concern was the presence of a region of supersonic flow near the slot downstream of the terminal shock. This concern was addressed by reducing the amount of turning at the end of the forward ramp such that any supersonic flow would not be allowed to expand, and so, accelerate.

A third item of concern was the presence of boundary-layer separation and reversed flow in the corner of the forward ramp and sidewalls near the slot. The solution was to add the slot corner porous bleed region as shown in Fig. 3. CFD simulations

demonstrated that with a reasonable amount of bleed flow, the separation could be significantly reduced. Inlet performance improved and the terminal shock appeared more focused.

A final item of concern was the interaction of the cowl shock and the sidewall near the cowl lip. The solution was to add the cowl sidewall porous bleed region as shown in Fig. 3. The bleed holes were drilled through the sidewall, and so, there was no plenum and the flow was essentially spilled. This bleed region was a passive porous bleed region driven by the lower static pressure of the external flow. CFD simulations indicated that the boundary-layer separation was significantly reduced. The cowl shock also moved closer to the cowl lip. The cowl sidewall bleed might also have enhanced sub-critical stability of the inlet (i.e. limit buzz cycles).

Bleed Optimization

A formal optimization procedure was applied to determine the set of bleed factors that optimized the performance of the inlet as measured by the maximization of the total pressure recovery. The bleed factors of interest were the bleed region porosity and plenum static pressure. With six bleed regions, this presented an optimization problem with 12 possible factors. Table 1 lists the bleed regions and factors.

Table 1. Bleed regions and factors.

Bleed Region	Type	Φ	p, psi
Ramp	Stability	40%	4.5
Sidewall	Stability	40%	4.5
Slot	Performance	100%	p_{slot}
Aft	Performance	Φ_{aft}	p_{slot}
Slot Corner	Performance	40%	p_{corner}
Cowl Sidewall	Performance	30%	1.0

Using the experience gained from the previous CFD simulations, the 12 possible bleed factors were reduced to 3 factors for the optimization study. The bleed factors for the ramp and sidewall bleed regions were first eliminated as factors. The ramp and sidewall bleed regions operate as stability bleed regions and should extract essentially no flow at the design condition for which the terminal shock is located downstream of these bleed regions. The porosity was specified at the baseline value of 40%. Over the course of previous CFD simulations, it was determined that a bleed plenum static pressure of 4.5 psi resulted in essentially no extracted flow; however, the boundary layers remained healthy over these bleed regions. The porosity of the slot bleed region was specified at 100% since this bleed region was not porous. The plenum static pressure of the slot bleed region (p_{slot}) was retained as a factor. The aft bleed region was directly connected to the slot plenum. The CFD simulations indicated that the slot plenum contained very low Mach number flow with a fairly uniform static pressure essentially equal to the slot bleed plenum static pressure. Thus, the aft bleed plenum static pressure was set equal to the slot bleed plenum static pressure. The porosity of the aft bleed region (Φ_{aft}) was retained as a factor. The porosity of the slot corner bleed region was specified at 40% to keep conditions uniform with the other porous bleed regions. The slot corner bleed plenum static pressure (p_{corner}) was retained as a factor. The cowl sidewall bleed region did not have a bleed plenum, but rather passively extracts the flow based on the static pressure of the external flow. To use the porous bleed model, the plenum static pressure was set equal to the external static pressure which was approximately 1.0 psi. This plenum static pressure was removed as a factor by assuming the external flow remained fixed. The porosity of the cowl sidewall bleed region was also removed as a factor and specified at 30%. Previous CFD simulations indicated that a porosity of 30% reduced the amount of bleed, which was essentially spilled, while still controlling adverse shock / boundary-layer interactions. Thus, the final set of factors were p_{slot}, p_{corner}, and Φ_{aft} as summarized in Table 1.

The formal optimization procedure involved determining the influence of the three bleed factors on the total pressure recovery and obtaining the set of factors that maximized the recovery. It was also recognized that interactions between the three factors were possible. The slot, slot corner, and aft bleeds were all located in the subsonic flow downstream of the terminal shock and acoustic communication between the bleed regions was possible. The influence and interaction of these three factors were examined statistically using methods of design of experiments (DoE) and response surface methodology (RSM).[5]

Applying the methods of DoE and RSM as part of a formal optimization procedure involved 1) defining the range over which to vary each factor, 2) defining the sets of factors at which to evaluate the recovery, 3) performing the CFD simulations for each set of factors, 4) statistically examining the variations in the recovery with respect to the factors, 5) formulating a quadratic response surface for the recovery, and 6) mathematically determining the optimum set of factors from the response surface equation.

The range for each of the three factors was selected based on knowledge of how the bleed rates varied as gained from previous CFD simulations. Further, the ranges were centered about the baseline values of the factors. It was decided to generate a quadratic response surface model which required three levels for each factor. Table 2 lists the baseline values of each factor along with the low and high values that define the factor range.

Table 2. Factors for the DoE study.

Factor	Baseline (psi)	Low (psi)	High (psi)
p_{slot}	4.0	3.5	4.5
p_{corner}	4.0	3.0	5.0
Φ_{aft}	30	20	40

With three factors and three levels, a full-factorial design would have involved 27 CFD simulations to determine the recovery for every combination of levels of the factors. The methods of DoE provided a statistical approach to generating the response surface with fewer CFD simulations. A central composite face–centered (CCF) design required only 15 CFD simulations. This reduction in the number of simulations was beneficial since it required several days to converge each simulation.

Ideally, the simulations should have been performed over a range of engine flows to generate a cane curve for each set of design factors. The optimization would then build a response surface based on the "knee" points of each cane curve. To reduce the number of simulations required, the study was performed assuming a constant engine flow of 90%. It was assumed that the cane curves had a similar shape with respect to the factors and the "knee" point occurred near the 90% engine flow. This assumption was likely not entirely valid; however, this assumption did lead to valid results for this study.

The total pressure recoveries obtained from the CFD simulations were then used to statistically construct a quadratic response surface using response surface methodology (RSM) with respect to the three factors. The Design Expert 6.0 software package was used to perform the statistical operations and build the quadratic response surface model.[6] The model building process started with a full quadratic model with respect to all three factors. Insignificant model terms were then eliminated starting with the most statistically insignificant. The resulting model only involved the factor p_{slot}. The resulting quadratic equation for the response surface was

$$Recovery = 0.88 - 0.048\frac{(p_{slot} - 4.0)}{0.5} - 0.030\left[\frac{(p_{slot} - 4.0)}{0.5}\right]^2.$$

The statistical model indicated that p_{corner} and Φ_{aft} were not significant factors in the behavior of the total pressure recovery over the range studied. This does not mean that the corner or aft bleed regions can be removed, rather, the change in the values of p_{corner} and Φ_{aft} over the range studied had no significant effect on the value of the total pressure recovery. Figure 5 plots the model over the range of p_{slot} and p_{corner}. Figure 5 indicates that the highest recovery is obtained when p_{slot} is approximately 3.5 psi. Further, the recovery "levels off", which indicates that reducing p_{slot} further, may not increase recovery by much.

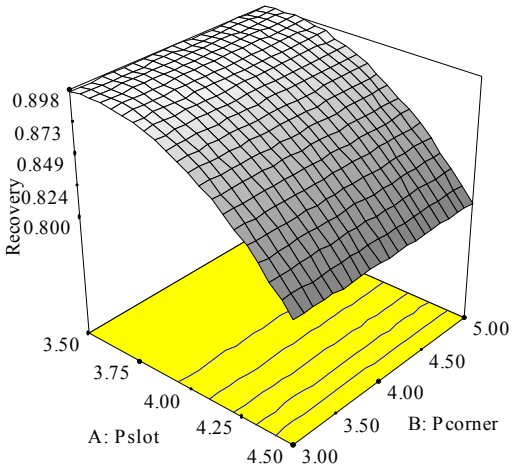

Figure 5. Response surface.

The quadratic equation was differentiated to obtain the mathematically optimum value of p_{slot} = 3.6 psi with the resulting total pressure recovery of 0.899. Given the flatness of the response, the value of p_{slot} = 3.5 psi was accepted as the optimum value with the resulting total pressure recovery from the quadratic equation of 0.898. The baseline values of p_{corner} and Φ_{aft} were chosen as the optimum values of those factors. The optimum set of values for the three factors are summarized in Table 3.

Table 3. Optimum set of values for factors.

Factor	Optimum Value
p_{slot}	3.5 psi
p_{corner}	4.0 psi
Φ_{aft}	30 %

CFD simulations were then performed using the optimized set of factors with the engine flow varied over a range of values to generate the cane curve. Figure 6 shows the comparison between the cane curve for the baseline and optimized values of the factors. At the 90% engine flow, the CFD simulation resulted in a total pressure recovery of 0.904 which compares well with the value of 0.898 from the quadratic equation. Figure 7 shows the comparison of the distortion index DPCPAV. The optimization procedures resulted in a significant increase in the inlet performance over the inlet with the baseline bleed factors, especially in the region of the "knee" of the cane curve.

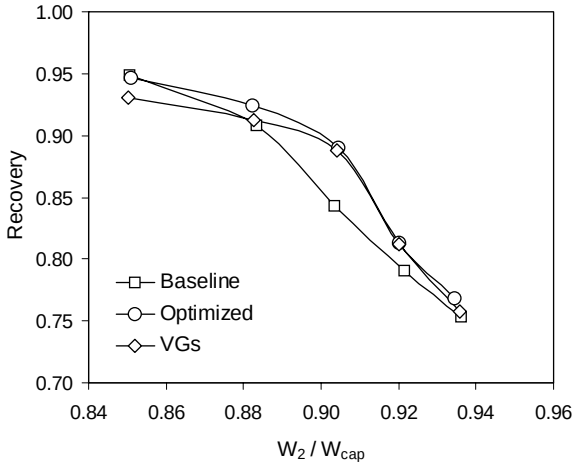

Figure 6. Cane curves.

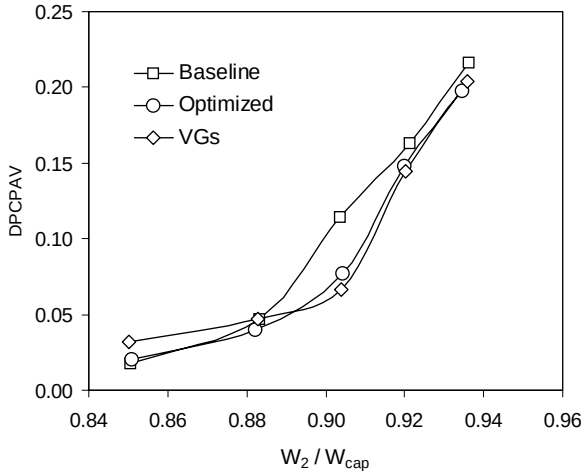

Figure 7. Distortion index DPCPAV.

Vortex Generators

CFD simulations were performed to examine the effect of an array of counter-rotating pairs of vortex generators (VGs) on the performance of the inlet. Figure 1 shows the position of the array, which spans the circumference of the subsonic diffuser. A cane curve was generated. Figure 6 compares the cane with VGs to the baseline and optimum cane curves. With the VGs installed, the recovery decreases at the lower engine flows, but is unchanged at the higher engine flows. At the lower engine flows, the flow in the subsonic diffuser is well-behaved (little boundary-layer separation), thus the VGs are not really needed and serve as a loss mechanism. At the higher engine flows there is significant boundary-layer separation on the top of the diffuser aft of the slot. However, the VGs are to be too far aft to be effective. The vortex generators did change the total pressure distribution at the engine face. The separated flow region moved from the top of the subsonic diffuser to the side. Figure 7 shows the variation of DPCPAV. At the "knee" of the curve, the distortion is about 14% lower than the simulation without VGs.

Slot and Cowl Lip Parametrics

CFD simulations were performed to examine variations in the inlet performance with respect to the various slot and cowl lip parametrics. CFD simulations were performed for five slot geometries and four cowl geometries for a total of 20 different inlet configurations. For each slot / cowl lip configuration, three different engine flows were simulated to obtain the portion of the cane curve near the knee of the curve. Thus, 60 CFD simulations were performed for this study. The CFD simulations did not indicate that any of the slot and cowl configurations provided significantly greater performance than the nominal slot and cowl lip configuration. The simulations did indicate that a few configurations where not worth examining during the wind tunnel tests. This information was made available during the wind tunnel tests as an aid in making efficient use of the costly wind tunnel resources.

Comparison between CFD and Experimental Data

The Parametric Inlet was fabricated and tested in the NASA-GRC 10-foot-by-10-foot supersonic wind tunnel (SWT). The main objective of the tests was to examine the performance of the inlet; however, the data also allowed examination of how well the CFD methods performed in predicting the performance. This section provides a preliminary comparison between the CFD and SWT data.

The inlet was connected to a cold pipe which had a translating conical plug assembly at its end. The test procedures involved setting the configuration of the inlet and then translating the mass flow plug in a stepwise manner to vary the cold pipe exit area, and so, vary the amount of engine flow (W_2) through the engine face. This provided a sweep of the engine flows. At each location of the plug, data were collected from the wall static pressure taps on the inlet surfaces and a 72-probe total pressure rake at the engine face.

A direct comparison between the CFD and SWT data was not possible because the flow conditions were slightly different. The CFD simulations were performed prior to the SWT tests and it was difficult to exactly match the CFD conditions in the SWT. Table 4 lists the flow conditions for the SWT and CFD data that are compared. Some of the differences in the flow conditions, such as the slot bleed rate, are considerable; however, the comparisons between the SWT and CFD data can provide a preliminary examination of how well the CFD simulations performed.

Table 4. Flow conditions for the wind tunnel (SWT) and CFD simulations.

	SWT	CFD
Mach	2.35189	2.35
Re (10^6)	2.50463	2.5
p_t (psi)	12.1242	11.7889
T_t (^oR)	559.799	550.0
Ramp bleed flow	0%	0%
Sidewall bleed	0%	0.03%
Slot and aft bleed flow	1.98%	3.30%
Corner bleed flow	1.06%	1.05%
Spillage flow	7.14%	5.19%
W_2/W_{cap}	0.89818	0.90428
Recovery	0.8734	0.8790

The comparison of static pressures on the inlet centerline of the forward and aft ramps and cowl between the CFD and SWT data is presented in Fig. 8. The experimental data plotted in Fig. 8 was for the flow conditions as listed in Table 4. The SWT data correspond to the point along the engine-flow sweep for which the static pressure at the engine face closely matched the static pressure at the engine face for the CFD data. The CFD data compare well on the forward ramp (up to x = 34 inches) where the flow is supersonic. Downstream of the terminal shock, the data does not compare well. The differences in flow conditions, especially bleed rates, may be the main factor for the differences. The static pressures on the cowl show good general agreement, especially in the initial turning between x34 and x42.

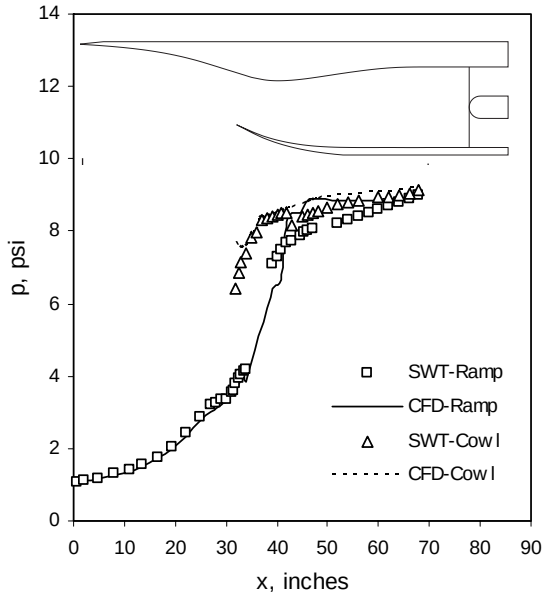

Figure 8. Wall static pressures on the inlet centerline along the forward and aft ramps and cowl.

The comparison of the cane curves for the CFD and SWT data is shown in Fig. 9. At first glance, the curves indicate considerable differences. Neither curve exhibits the characteristic vertical portion of the cane that indicates that the terminal shock is supercritical and has entered the duct with choked flow. In the CFD simulations, the terminal shock did not completely enter into the duct, and so, the duct did not reach a choked condition. For the experimental data, it is known that the engine flow measurements lose accuracy at the higher engine flows when the flow chokes or there exists extensive boundary-layer separation; and so, there appears uncertainty in the results, which needs to be examined. In the region of the "knee" of the cane curves, the comparison between the test data and the CFD is reasonable. The solid circles in Fig. 9 indicate the two points listed in Table 4. The differences in the flow conditions and bleed rates likely cause some of the differences in the recovery and engine flow plotted in the cane curves of Fig. 9. However, the trends between the recovery and the engine flow plotted in the "knee" of the cane curves are similar.

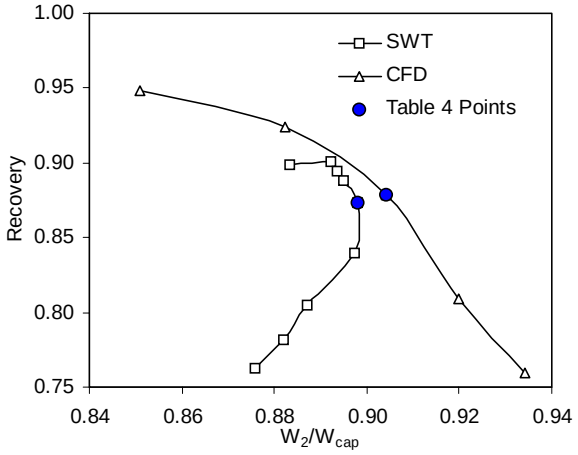

Figure 9. Cane curves.

The total-pressure distributions at the engine face for the CFD and SWT data are presented in Fig. 10. The CFD data was interpolated to the probe locations of the 72-probe total pressure rake. A direct match is not expected due to differences in the flow conditions and bleed rates. However, the trend of the distributions is similar with the low-total-pressure regions at the top of the subsonic diffuser and high-total-pressure regions at the bottom of the diffuser. Further, the range of contour lines is approximately the same.

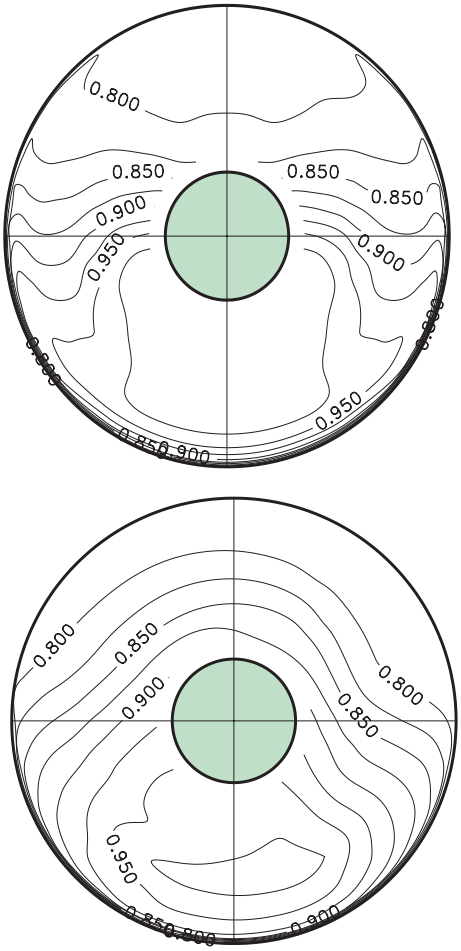

Figure 10. Total pressure contours at the engine face from CFD (top) and SWT (bottom).

Conclusions

CFD played a major role in the design of the Parametric Inlet. The ability to simulate turbulent flows with shock / boundary-layer interactions highlighted several problems with the shape and bleed systems of the inlet that would have been difficult or impossible to predict using traditional design methods. Optimization methods based on the design of experiments (DoE) and response surface methodology (RSM) demonstrated effectiveness for supersonic inlet design. The preliminary comparisons between the experimental and CFD data are encouraging; however, given the differences in flow conditions, the comparisons do not validate the CFD methods. Further CFD simulations will be conducted as part of a formal validation study. This will build confidence in the use of CFD methods and will also highlight weaknesses in the CFD methods, which will lead to improvements that will enhance the capability of NASA and USA industry to simulate and design supersonic inlets.

References

[1] Plencer, R.M., A. Misra, E.J. Graber, R.J. Shaw, and G.T. Seng, "Engine Technology Challenges for the High-Speed Civil Transport Plane," AIAA Paper 1998-2505, June 1998.

[2] Society of Automotive Engineers (SAE), "Gas Turbine Engine Inlet Flow Distortion Guidelines," SAE ARP 1420, Rev. B, February 2002.

[3] Mani, M., A. Cary, and S. Ramakrishnan, "A Structured and Hybrid-unstructured Grid Euler and Navier-Stokes Solver for General Geometry," AIAA-2004-0524, January 2004.

[4] Slater, J.W., "CFD Methods for Computing the Performance of Supersonic Inlets," AIAA-2004-3404, July 2004.

[5] Montgomery, D.C., Design and Analysis of Experiments, John Wiley & Sons, Inc., New York, 2001.

[6] State-Ease, Inc. www.stat-ease.com. April 2005.